AFRL-RQ-WP-TP-2013-0062

EXAMINING PASSIVE FLOW CONTROL DEVICES WITH HIGH SPEED SHADOWGRAPH IMAGES AROUND A MACH 1.5 CAVITY FLOW FIELD (POSTPRINT)

Ryan F. Schmit, Frank Semmelmayer, Mitchell Haverkamp, and James E. Grove

Integrated Systems Branch
Aerospace Vehicles Division

Anwar Ahmed

Auburn University

JUNE 2012

AIR FORCE RESEARCH LABORATORY
AEROSPACE SYSTEMS DIRECTORATE
WRIGHT-PATTERSON AIR FORCE BASE, OH 45433-7542
AIR FORCE MATERIEL COMMAND
UNITED STATES AIR FORCE

REPORT DOCUMENTATION PAGE

Form Approved
OMB No. 0704-0188

1. REPORT DATE *(DD-MM-YY)*	2. REPORT TYPE	3. DATES COVERED *(From - To)*
June 2012	Conference Paper Postprint	01 January 2010 – 01 January 2012

4. TITLE AND SUBTITLE
EXAMINING PASSIVE FLOW CONTROL DEVICES WITH HIGH SPEED SHADOWGRAPH IMAGES AROUND A MACH 1.5 CAVITY FLOW FIELD (POSTPRINT)

5a. CONTRACT NUMBER
In-house

5b. GRANT NUMBER

5c. PROGRAM ELEMENT NUMBER
62201F

6. AUTHOR(S)
Ryan F. Schmit, Frank Semmelmayer, Mitchell Haverkamp, and James E. Grove (AFRL/RQVI)
Anwar Ahmed (Auburn University)

5d. PROJECT NUMBER
2404

5e. TASK NUMBER
N/A

5f. WORK UNIT NUMBER
Q08B

7. PERFORMING ORGANIZATION NAME(S) AND ADDRESS(ES)
Integrated Systems Branch (AFRL/RQVI)
Aerospace Vehicles Division
Air Force Research Laboratory, Aerospace Systems Directorate
Wright-Patterson Air Force Base, OH 45433-7542
Air Force Materiel Command, United States Air Force

Auburn University
Auburn, AL

8. PERFORMING ORGANIZATION REPORT NUMBER
AFRL-RQ-WP-TP-2013-0062

9. SPONSORING/MONITORING AGENCY NAME(S) AND ADDRESS(ES)
Air Force Research Laboratory
Aerospace Systems Directorate
Wright-Patterson Air Force Base, OH 45433-7542
Air Force Materiel Command
United States Air Force

10. SPONSORING/MONITORING AGENCY ACRONYM(S)
AFRL/RQVI

11. SPONSORING/MONITORING AGENCY REPORT NUMBER(S)
AFRL-RQ-WP-TP-2013-0061

12. DISTRIBUTION/AVAILABILITY STATEMENT
Approved for public release; distribution unlimited.

13. SUPPLEMENTARY NOTES
PA Case Number: 88ABW-2012-3319; Clearance Date: 11 June 2012. This technical paper contains color.

All references in this report to Air Force division AFRL/RB refer to AFRL/RQ; AFRL/RB and another division merged into AFRL/RQ during this effort.

Conference paper presented at the 6th AIAA Flow Control Conference, 25 - 28 June 2012, New Orleans, Louisiana.

14. ABSTRACT
An examination of a rectangular cavity with an L/D of 5.67 was tested at Mach 1.5 with a corresponding Reynolds number of 2.3×10^6/ft. High speed shadowgraph movies were simultaneously sampled with dynamic pressure sensors at 75 kHz. Fourier analysis was performed on the high speed movies as well as the dynamic pressure data, which resulted in determining the locations of dominant cavity frequencies in the flow field. Four passive flow control devices were tested, two of which have historically preformed well, while two neither reduced the main acoustic tones nor reduced the broadband levels. From the high speed shadowgraph movies, observations are made in the changes in the cavity flow physics when the passive flow control devices are used, and will be discussed.

15. SUBJECT TERMS
cavity, flow control, Fourier analysis, acoustics

16. SECURITY CLASSIFICATION OF:			17. LIMITATION OF ABSTRACT:	18. NUMBER OF PAGES	19a. NAME OF RESPONSIBLE PERSON (Monitor)
a. REPORT	b. ABSTRACT	c. THIS PAGE			Ryan F. Schmit
Unclassified	Unclassified	Unclassified	SAR	26	19b. TELEPHONE NUMBER *(Include Area Code)* N/A

6th AIAA Flow Control Conference
25 - 28 June 2012, New Orleans, Louisiana

AIAA 2012-3139

Examining Passive Flow Control Devices with High Speed Shadowgraph Images around a Mach 1.5 Cavity Flow Field

Ryan F. Schmit[1], 1st LT Frank Semmelmayer[2], 2nd LT Mitchell Haverkamp[3], James E. Grove[4]

U.S Air Force Research Laboratory, Wright-Patterson Air Force Base, OH 45433, USA

and

Anwar Ahmed[5]

Auburn University, Auburn AL, USA

An examination of a rectangular cavity with an L/D of 5.67 was tested at Mach 1.5 with a corresponding Reynolds number of $2.3x10^6$/ft. High speed shadowgraph movies were simultaneously sampled with dynamic pressure sensors at 75 kHz. Fourier analysis was performed on the high speed movies as well as the dynamic pressure data, which resulted in determining the locations of dominant cavity frequencies in the flow field. Four passive flow control devices were tested, two of which have historically preformed well, while two neither reduced the main acoustic tones nor reduced the broadband levels. From the high speed shadowgraph movies, observations are made in the changes in the cavity flow physics when the passive flow control devices are used, and will be discussed.

Nomenclature

D	=	Cavity Depth
f	=	frequency
I	=	Image Intensity
k	=	Convection Velocity
L	=	Cavity Length
M	=	Mach Number
m	=	Mode Number
N	=	Number of Sample Blocks
n	=	Sample Size
OASPL	=	Overall Sound Pressure Level
P	=	Pressure
P_{ref}	=	Reference Pressure
Q	=	Dynamic Pressure
S	=	Spectrum Level
SR	=	Sample Rate
SPL	=	Sound Pressure Level
U_∞	=	Freestream Velocity
W	=	Cavity Width
x	=	Free-stream Direction
y	=	Wall-Normal Direction
z	=	Span-wise Direction
γ	=	Correction Factor

[1] Aerospace Engineer, AFRL/RBAI, 2130 8th Street, Associate Fellow AIAA
[2] Test Engineer, AFRL/RBAX, 2130 8th Street
[3] Test Engineer, AFRL/RBAX, 2130 8th Street
[4] Weapons Integration Team Lead, AFRL/RBAI, 2310 8th Street,
[5] Professor, Aerospace Engineering Department, Associate Fellow AIAA

This material is declared a work of the U.S. Government and is not subject to copyright protection in the United States.

I. Introduction

For over 60 years, weapon bays, landing gear, and other similar cavities has been examined by numerous researchers throughout the world. Starting from the early work by Roshko, Rossiter and others, the researchers have used theoretical and experimental modeling to examine and understand the flow physics that occur inside the cavity at various length to depth ratios, Mach and Reynolds numbers.

Rossiter[1] was the first to produce a theoretical model from experimental data for the cavity. After examining shadowgraph photographs along with acoustic pressure sensors for varying cavity length to depth ratios (L/D) of 2 to 10, he produced his now famous semi-empirical equation:

$$\frac{fl}{U_\infty} = \frac{m-\gamma}{M+\frac{1}{k}} \tag{1}$$

which is based on the shedding frequency and convection velocity of the shear layer, the freestream Mach number and the length of the cavity. This model initiated the beginning of the understanding of the flow physics inside the cavity.

Heller and Bliss[2] examined the cavity using a water table and showed the motion of the acoustic waves traversing back and forth inside the cavity, as well as the radiation of the acoustic waves outside the cavity. Tam and Block[3] used simulated point sources at the trailing edge of the cavity to show acoustic wave paths that form inside and outside of the cavity. Zhuang et al.[4] used a 1 kHz shadowgraph system to examine the cavity and described the five different waves that were present in their images. Moon et al.[5] examined a cavity with high speed schlieren and confirmed the five different waves that Zhuang et al. observed. Moon et al. observed the acoustic wave motion inside the cavity, identified its precise motion, and calculated its frequency to be near the first fundamental frequency of their cavity. Schmit et al.[6] examined the cavity that is present in this paper, using high speed shadowgraph simultaneously sampled with dynamic pressure, and showed all the mechanisms that control the cavity from the tripping of the shear layer vortices, the entrainment waves impacting the aft wall, to the motion of multiple acoustic wave traversing the cavity ceiling.

Once Computational Fluid Dynamics (CFD) became prevalent, numerous researchers have studied the cavity to understand the flow physics around two and three dimensional rectangular cavities including Rizzetta[7], Peng[8] Li et al.[9] Li et al. used an Implicit Large Eddie Simulation (ILES) to examine a Mach 2.0 L/D = 2 cavity and showed the compression waves and cavity tones inside the cavity and how they interacted to create the feedback mechanism inside the cavity.

For the past fifteen years, experimental and computational computing power has become phenomenal and an ally to all fluids research. With the advent of PIV, several studies have examined the cavity. Murray and Ukeiley[10], Dudley and Ukeiley[11], Koschatzky et al.[12] have shown discreet physics of the flow field, mainly on the centerline of the cavity and the shear layer.

Since Rossiter reducing the cavity tone and the broad band noise through the use of geometry modification and flow control has become an important objective of cavity research. A review paper by Cattafesta et al.[13] outlines work of numerous researchers who have examined the effects of geometric modification, active flow control and feedback flow control techniques applied to cavity flows. All have shown some success at reducing either cavity tones, the broad band noise or both.

As with the recent work using this cavity model by Schmit et. al[6, 14], the intent of this research is to examine the fundamental differences between the cavity flow physics using four different geometry modifications which have been used on prior experimental and computational research but have had temporal and visualization limitations. By understanding the subtle differences in the flow physics between the geometry modifications, new actuators and control methodologies can be developed to take advantage of the flow physics to reduces the cavity tones as well as the broadband noise to levels suitable for future aircraft weapons bays.

II. Experimental Setup

A. Trisonic Gasdynamics Facility

The Trisonic Gasdynamics Facility (TGF) shown in Figure 1 is located on Area B of Wright-Patterson Air Force Base. The tunnel was built in the 1950's to provide researchers a wind tunnel to study complex flow configurations in the sub and supersonic regime within the Air Force and DoD organizations. When coupled and synchronized, the 3500 HP and 5000 HP motors provide the power to this closed circuit wind tunnel to achieve subsonic velocities from Mach 0.23 to 0.87, and discrete supersonic Mach numbers of 1.5, 1.9, 2.3 and 3.0 with interchangeable nozzle blocks. The test section total pressure is adjustable from 0.5 to 2.0 atmospheres. The

maximum subsonic Reynolds number for the tunnel is 2.5 million per foot and the maximum subsonic dynamic pressure is 350 psf. The maximum supersonic Reynolds number is 5 million per foot and the maximum supersonic dynamic pressure is 1000 psf. The stagnation temperature is held constant at 75°F.

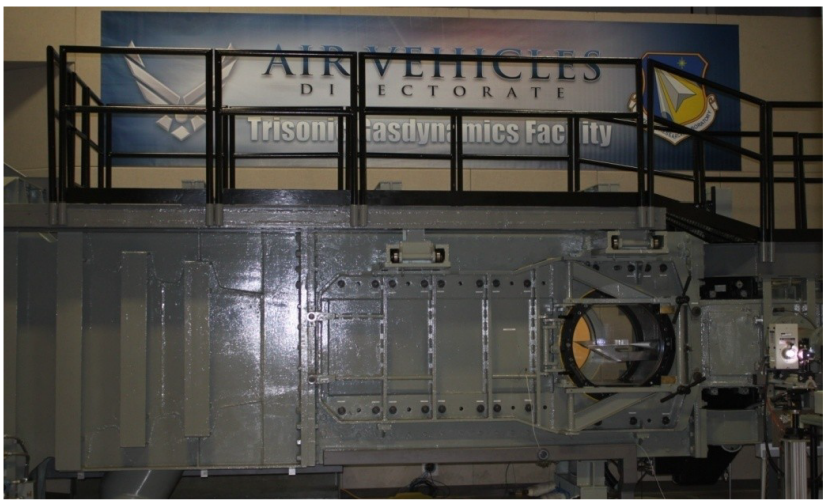

Figure 1. Trisonic Gasdynamics Facility

The test section is two feet high, two feet wide and four foot long with two optically flat 26 inch diameter viewing windows on either side of the test section. The primary model support is a crescent mounted sting, which can be used to reach various attitudes, or model orientations, including pitch from -1° to +18.5°, roll from -90° to +180°. Refer to the TGF User's Manual[16] for more information and capabilities.

B. Optical Turbulence Reduction Cavity Model

The original Turbulence Reduction Cavity model was tested several times from the mid 1970's to the late 1980's, and provided acoustic measurements and oil flow visualization inside the cavity as well as Schlieren photographs of the flow field outside of the cavity. At the time, these diagnostic techniques were still state of the art, though they had been around for a few decades[17]. With the subsequent development of state of the art non-intrusive flow field measuring techniques, i.e. Particle Image Velocimetry (PIV), Laser Doppler Anemometry (LDA) and Planar Induced Florescence (PLIF), the original Turbulence Reduction Cavity would not provide the necessary optical access for said techniques.

Therefore, a new Optical Turbulence Reduction Cavity model was built for the TGF. Figure 2 shows the new model inside the TGF. The cavity dimensions are: length 8.5 inches, depth 1.5 inches and width 2.5 inches, the L/D is 5.67 and the model scale is approximately 1/20th. The fore body of the model is 7.0 inches long and is 5 inches wide.

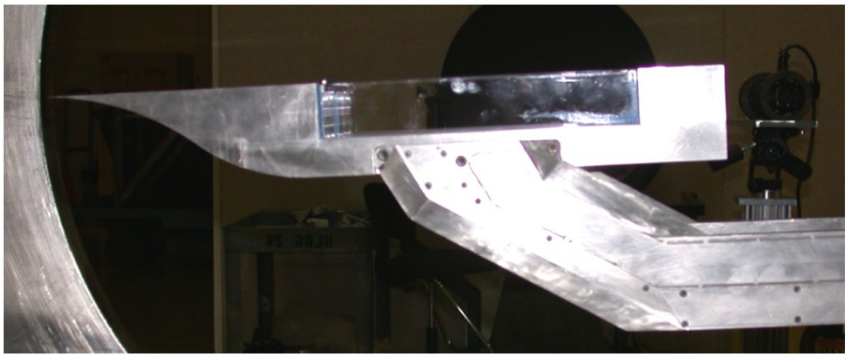

Figure 2. The Optical Turbulence Reduction Cavity mounted inside the TGF

The forward and aft wall blocks of the cavity are designed to be replaceable so that both passive and active flow control devices are easy to insert without compromising overall geometry of the cavity during testing. This paper will cover results for the cavity at Mach 1.5 at a Reynolds numbers of 2.3 million per foot.

To ensure an attached boundary layer along the fore body the cavity, the pitch angle was set to +3/4°. There are two methods to set the pitch angle for this model, at the tunnel support crescent and/or at the sting knuckle joint. The knuckle joint, shown in Figure 3, is need because the crescent does not have yaw capability when the model is rolled 90°. When the cavity roll angle is 0°, i.e. looking across the cavity as shown in Figure 2, the crescent is adjusted to set the pitch angle to +3/4°, while the knuckle joint is set to 0°. When the cavity is rolled 90°, i.e. the cavity ceiling is normal to the tunnel windows, the crescent angle is set to 0° while the knuckle joint sets the pitch angle to +3/4°.

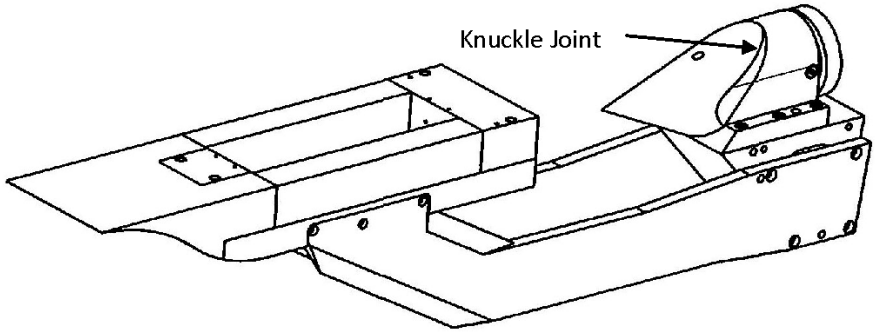

Figure 3. Isometric sketch of the Optical Turbulence Reduction Cavity Model

As mentioned earlier, the cavity model was built with non-intrusive diagnostic techniques in mind, therefore there are three interchangeable optical quality fused silica windows for this model. The two side walls, as shown in Figure 2, are replaceable with two aluminum blanks if required. The ceiling window is interchangeable with an aluminum blank, as shown in Figure 4, that contains 2 thermocouples, 5 static pressure ports and up to 7 dynamic pressure sensors. For this test, 5 of the 7 dynamic pressure sensors were properly working. Four more dynamic pressure sensors were located in the aft block, 2 on the aft wall and 2 on the waterline downstream of the cavity. Table 1 shows the location of all working dynamic pressure sensors.

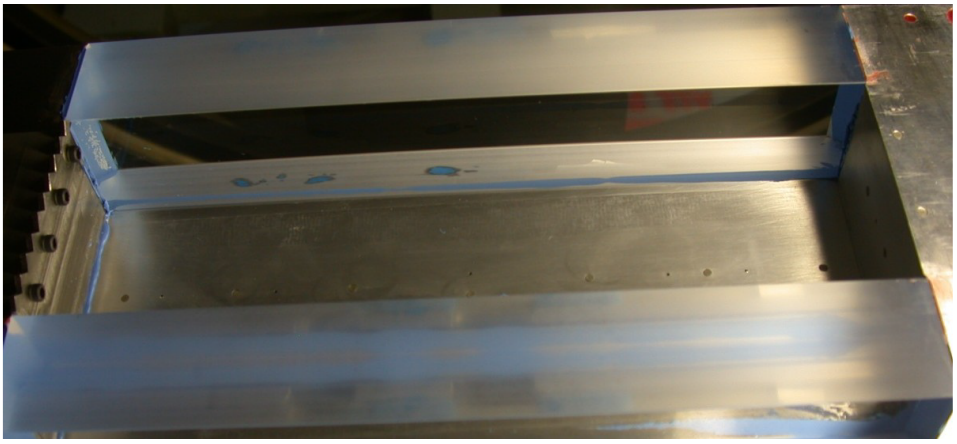

Figure 4. View inside the cavity with mounted sensors

Table 1: Locations of Dynamic Pressure Sensors

Sensor	x/L	y/D	z/W
Mic 1	0.05	-1.00	0.00
Mic 2	0.20	-1.00	0.00
Mic 3	0.35	-1.00	0.00
Mic 4	0.65	-1.00	0.00
Mic 5	0.80	-1.00	0.00
Mic 6	0.95	-1.00	0.00
Mic 7	1.02	0.00	-0.20
Mic 8	1.00	-0.50	-0.16
Mic 9	1.02	0.00	0.20
Mic 10	1.00	-0.50	0.16

C. Geometry Modifying Control Devices

In applying control methodologies to cavity flows, both the state of the approaching boundary layer prior to separation, and the separated turbulent shear layer play an important role in cavity acoustics. It has been shown that the streamwise scales of turbulence decrease significantly in the supersonic turbulent boundary layer[18], and likewise the compressibility tends to reduce the spread of shear layer [19,20] resulting in a reduction in the Reynolds stresses and entrainment[21]. However the wavelength and intensity of the acoustic waves are much larger than the turbulence scales[22].

For an inviscid shear layer the results of Blumen et. al[23] show that compressibility also prevents the growth of Kelvin-Helmholtz modes and their interactions. For flow control applications, it is therefore important to introduce known disturbances of relatively high amplitude to offset the dampening of the secondary structures in the post-separated shear layer. Consequently the edge tones thus produced by the shear layer impinging on the rear corner of the cavity will retain energy in the lower wave number range. Experiments by Papamoschou and Roshko have clearly shown that the spread rate of the turbulent shear layer largely depended on the Mach number and is independent of the transverse density gradients[24].

Recently Schulin and Trofimov reported that the vorticity generated by supercritical elements such as dots and triangular prisms placed in a supersonic turbulent boundary layer survived up to 10^4 times the height of the generators, and the disturbances amplified in the presence of adverse pressure gradient[25]. This shows the effectiveness of passive flow control techniques.

The passive flow control devices are broadly categorized as those applied to the leading edge and the trailing edge of a cavity. Leading edge devices include spoilers, wedges, cylinders, etc. and are primarily intended for the thickening of the separated shear layer[26,27]. The trailing edge treatment on the other hand is designed to deflect the shear layer and or acoustic wave by shaping of the rear wall[28].

For the present experiments, the passive devices consisted of the flat spoiler, a large 3D backward facing step, ridges and 6 mm Rod at the leading edge. The theory behind all of the passive control device will be explained below.

One of the oldest known and used geometry modifying control devices is the flat spoiler that spans width of the cavity and is shown in Figure 5a. The flat spoiler is 2.5 inches wide, protrudes 0.160 inches above the cavity waterline and is 0.063 inches thick. The theory as to why the flat spoiler works is that it lofts the boundary layer over the cavity, reducing the shear layers ability to penetrate the cavity depths[26].

The next three devices tested use a similar methodology. When the boundary layer separates at the edge of a back step, the vorticity in the separated boundary layer rolls up and forms streamwise vortices at the base of the V-groove [29]. Since the vortices in the base of the V-groove are very stable[30], they introduce streamwise vorticity in the shear layer resulting in thickening of the shear layer due to entrainment and introduce oblique disturbances as they are more unstable [31]. Figure 5b and 5c show the small and large 3D backward facing step, respectively. The four V-shaped cuts are 2.5 inches wide and extend 0.5 inches or 1 inches upstream and are 4mm deep. These plates are used to introduce streamwise vortical structures in the shear layer and the resulting flow field from these devices are depicted in Figure 5d.

Figure 5e shows another V-shaped device with streamwise grooves of 60 degrees interior angle with depth on the same order of the boundary layer displacement thickness. Again streamwise vortex pairs are depicted in Figure 5e. In this paper this device is named Ridges.

The last geometry modifying control device is the rod in a cross flow, and is shown in Figure 5f. The 6 mm diameter ceramic rod is 2.5 inch wide and the gap between the rod and the cavity waterline is 2.54 mm. The rod is held in position using two 8 mm diameter vertical posts. The gap between the rod and the cavity waterline is adjustable using set screws. Stanek[27] describes the development and theory behind the rod in a cross flow as it pertains to a high frequency flow control device. The rod's basic theory is that the shedding produced by the rod does not enable large coherent vortices to form downstream, resulting in suppression. The basic parameters for the rod are: the diameter is only 2/3 the boundary layer thickness, the gap distance should be 2/3 the boundary layer thickness.

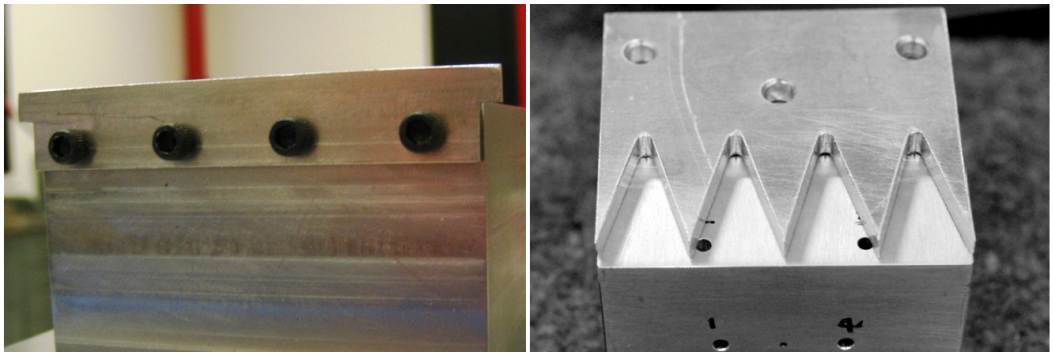

a. b.

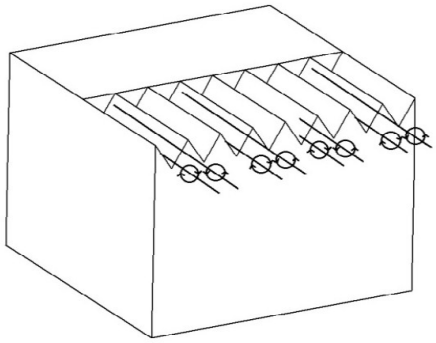

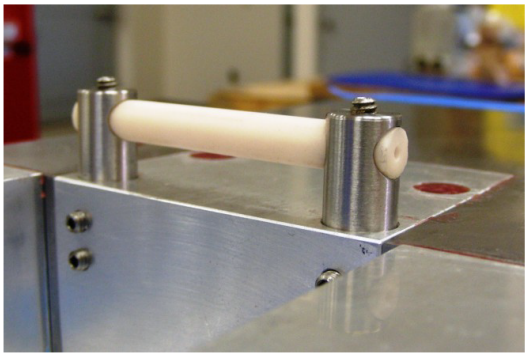

c. d.

Figure 5: The geometry modify flow control devices, a. Flat Spoiler, c. Large 3D backward facing step, e. Ridges, f. 6 mm Rod.

D. Shadowgraph Setup

Shadowgraph photography is one of the oldest non-intrusive flow diagnostic techniques available in the TGF. For more information about this technique please refer to Settles[32]. The shadowgraph setup in the TGF is a standard Z-type. A 350 Watt arc lamp is used as the light source, located in the test area, and is shown in Figure 6a. The light reflects off the test area's parabolic mirror, passes through the TGF test section, then through the control room window, where it finally reflects off the control room's parabolic mirror. Once the light arrives onto the optical table, see Figure 6b, it encounters a 50/50 plate beam splitter that is set at approximately 45° to the light's path. The reflected light from the plate beam splitter is used for data acquisition. The light that passes through the plate beam splitter is used to monitor tunnel condition using a 30Hz astronomy camera with a 35mm lens. Because of the sensitivity of the astronomy camera, several neutral density filters are used to reduce the light intensity prior to reaching the vertical knife edge. The tunnel and model windows were cleaned as needed.

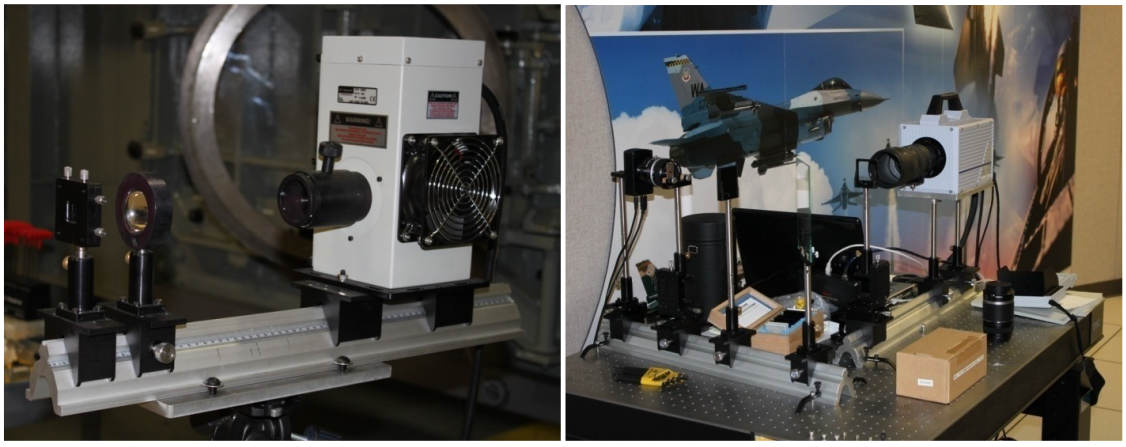

a. b.

Figure 6. Shadowgraph Optical Components. a. Light source with collimating optics. b. Receiving optics and cameras

A Photron FASTCAM SA1 with an AF Zoom-NIKKOR 80-200 mm f/2.8D ED lens was used to capture the shadowgraph images. Because of the amount of light lost by a knife edge, the FASTCAM was setup for shadowgraph imaging. The camera's frame rate was set to 75000 Hz which provides a maximum resolution of 512 pixels horizontally by 128 pixels vertically. The electronic shutter speed was 1/2,700,000 sec., or 0.37 μsec. The pixel depth for this camera is 2^8 with three channels of color, RGB.

E. Data Acquisition and Analysis

The thermocouple data was sampled at 1 kHz, averaged, and recorded at 5 Hz using a National Instruments Data Acquisition card. The static pressure data was acquired with a Pressure Systems Model 8400 Scanner, at 100 Hz, averaged, and also recorded at 5 Hz. Both the temperature and static pressure sensors were check-calibrated in the model and have an uncertainty of 0.1% FS and 0.1% FS respectively. The dynamic pressure sensors were check-calibrated in the model and have an error uncertainty of 1.0% FS.

The dynamic pressure sensor data were acquired using the RBAX high-speed data (Whisper) system. This system performed simultaneous sample-and-hold acquisition at a rate of 75 kHz for data records 2 seconds in length. Digital images were simultaneously acquired during several dynamic pressure acquisition cycles. To accomplish image acquisition, a 5 V TTL trigger signal was sent from the high speed data acquisition system to the FASTCAM digital camera. The entire 2 seconds of high speed video was kept for only a handful of test points, since the ".avi" movie file size was 27.4 GB. For all other test points the first 5000 images were kept, which results in an ".avi" movie file size of just under 1GB. For the dynamic pressure data, each channel was 150,000 samples were collected.

A Discrete Fourier Transform (DFT) was used to convert the blocks of dynamic pressure and shadowgraph video data into the frequency domain. Prior to the DFT of the shadowgraph video, each pixel was converted from RGB to grayscale using Eq. (2).

$$\mathbf{I = 0.2989I(R,0,0) + 0.5870I(0,G,0) + 0.1140I(0,0,B)} \tag{2}$$

where I is the intensity of each pixel and R, G, and B is the individual intensity values for each of the color channels, Red, Green and Blue. The mean grayscale intensity was removed and one block of 4096 images was analyzed giving a δf of 18.31 Hz. Further analysis on the video images was not preformed.

Each dynamic pressure sensor was split into 37 blocks of 4096 samples resulting in a δf of 18.31 Hz. After determining the amplitude of the transformed pressure signal, the mean pressure amplitude is converted into sound pressure level using Eq. (3).

$$\mathbf{SPL(f) = 20Log_{10}\left(\frac{\sum_{i=1}^{n} PA_i(f)}{nP_{ref}}\right)} \tag{3}$$

where P_{ref} is 2.9e-9 psi and n is the number of blocks.

Since the sample frequency and consequently the DFT doesn't have an ideal response characteristic with a bandwidth of 1 Hz the sound pressure level needs to be converted to spectrum level using Eq. (4).

$$\mathbf{S(f) = SPL(f) + 10Log_{10}\left[\frac{SR}{N}\right]} \tag{4}$$

where SR is the sample rate. To calculate the overall pressure level, the spectrum level is converted back to pressure using Eq. (5).

$$\mathbf{P(f,Q) = P_{ref}10^{\frac{S(f,Q)}{20}}} \tag{5}$$

Then the overall spectrum level, Eq. (6)., is determined by integrating the pressure over the frequency spectrum and converting it back to a spectrum level.

$$\mathbf{OASPL(f,Q) = 20Log_{10}\left[\frac{\sqrt{\sum P(f,Q)^2}}{P_{ref}}\right]} \tag{6}$$

III. Results

The results shown in this paper are for freestream Mach number of 1.5 and Reynolds number of 2.3×10^6. The baseline results shown in this paper are from Schmit et al. [6] and are used for comparison purposes in this paper.

Figure 7 shows the acoustic spectrum at the aft wall of the cavity along with four geometry modifying control devices that were tested. Though several more geometry modifying devices where tested at this condition the four that will be discussed in this paper show a performance extreme in the acoustic results and therefore a detailed analysis on the effects to the flow physics will be discuss. The best geometry modifying device that reduced the acoustic tones and the broadband noise level the most is and 6 mm Rod with a 2.54 mm gap. The next best performing geometry modifying device was the large 3D backward facing steps. It was able to reduce the acoustic tone significantly, but slight increased or maintained the broadband noise throughout the spectrum. The flat spoiler was able to reduce the broadband noise though it could not reduce the acoustic peaks to the broadband levels like the 6 mm rod. The Ridges devices was the worst performing device which increased the broadband noise level and dramatically increase the acoustic tone and frequency shift the acoustic tone by 50 Hz lower. Table 2 shows the acoustic performance of each of the passive devices tested and compared to the baseline.

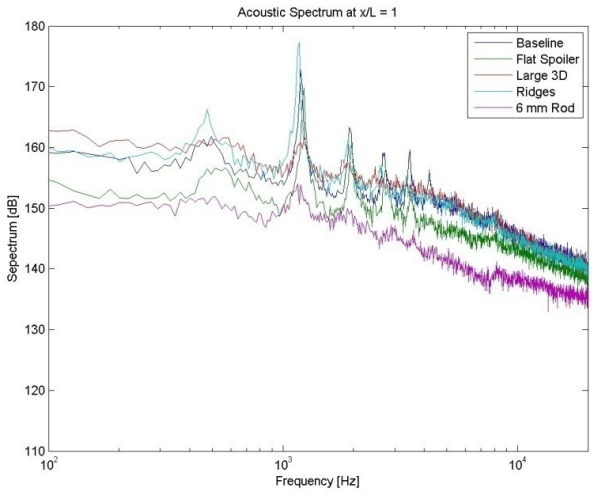

Figure 7. Aft wall pressure spectrum for various passive flow control devices

Table 2. Acoustic tone reduction and shift results.

Device	OASPL dB	Delta OASPL dB	Peak Frequency Hz	Peak Tone dB	Delta Peak Tone dB
Baseline	182.58		1190	172.8	
Flat Spoiler	179.18	3.4	1227	169.8	3.0
Large 3D Step	181.65	0.93	585.9 and 1227	161.1	11.7
Ridges	184.17	-1.59	1172	177.3	-4.5
6 mm Rod	173.80	8.78	1154 and 1190	153.9	18.9

Figure 8 shows five instantaneous images of the side view of the cavity at Mach 1.5. Figure 8a is the baseline image that has previously been shown in Schmit et al.[6] and is used for a comparison with other images. The shocks seen in the inside the cavity are really outside of the model and do not influence the inside cavity flow field patterns, for a better description of where these shock come from see Schmit et al.[6]. Figure 8b shows the flat spoiler image which has been zoomed in to match the other images view point in this figure and therefore is a lower quality image. Even so it can be seen that there is a shock off the flat spoiler and it lifts the shear layer slightly. The flat spoiler does delay the shear layer from producing a large scale vortex but the vortex still penetrates the cavity flow field which in turn influence the acoustic wave production. At this instantaneous image an aft ward traveling acoustic wave is noticeable inside the cavity. Figure 8c shows the Ridges device image and there is little difference between the baseline can be noticed. There is an expansion fan created by the step at the leading edge of the device that is observable in the image. The initial shear layer, just off the leading edge of the cavity is closer to the waterline of the cavity mainly due to the fact that the Ridges device is below the waterline of the cavity as well. Again an aft ward traveling acoustic wave is noticeable inside the cavity. Figure 8d shows the large three dimensional backward facing steps image. Streamwise vortices are produced from the large three dimensional backward facing steps and are noticeable below the leading edge of the cavity. Large scale vortices formation are not easily observable along with acoustic waves inside the cavity. Figure 8e shows the 6mm Rod image and the wake of the rod is clearly seen. Again no larger scale vortices formation are noticeable but the wake of the rod does penetrate the cavity depths more significantly than in the subsonic case[14]. No acoustic waves are observable as well as flow field inside the cavity.

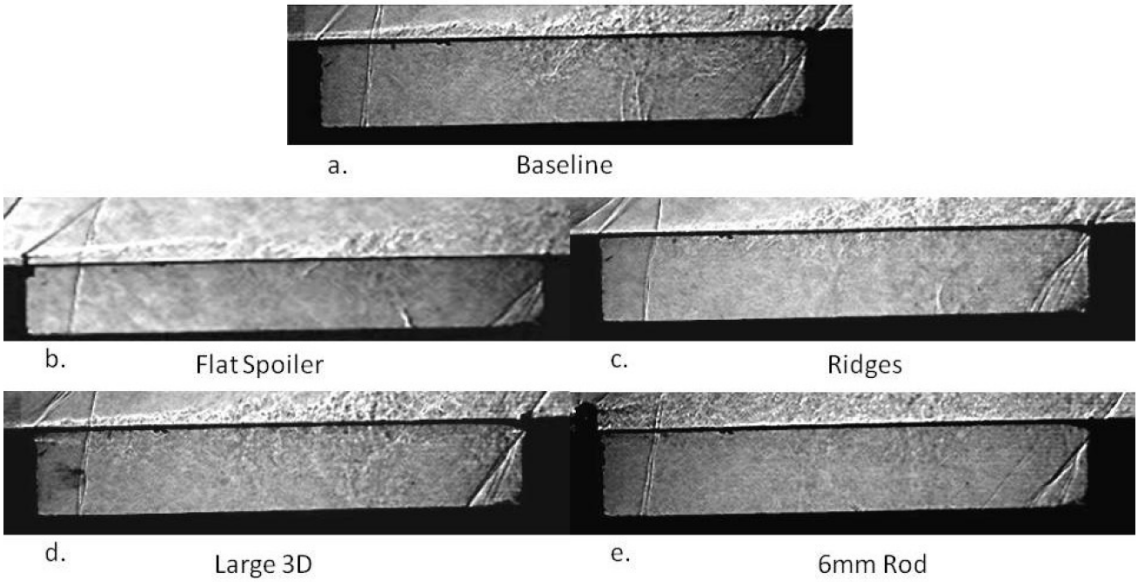

Figure 8 Shadowgraph Images of the side view a. Baseline, b. Large Backward Facing Steps, c. Ridges, d. Flat Spoiler, e. 6 mm Rod.

Figure 9 shows five instantaneous images of the top view of the cavity at Mach 1.5. Faint diamond patterned shocks are observable in all of Figure 9's images, these shocks are from the bifurcated arms the support the model. Figure 9a. is the baseline image and again is used for a comparison with other images. One interesting

observation in the baseline image is the aft ward traveling wave that stretches across the entire cavity. Figure 9b, c, d, and e shows the flat spoiler, ridges device, large three dimensional backward facing step and the 6 mm Rod, respectively. In the top view most flow structures are not observable as compared to the side view, but by understanding how the flow control device changes the flow field an better understand of the side view images can become more clear. The aft ward traveling acoustic wave can be clearly observed in Figure 9c but all of the images have an acoustic wave in the images, e.g. nearly straight lines across the cavity, except for the 6 mm Rod.

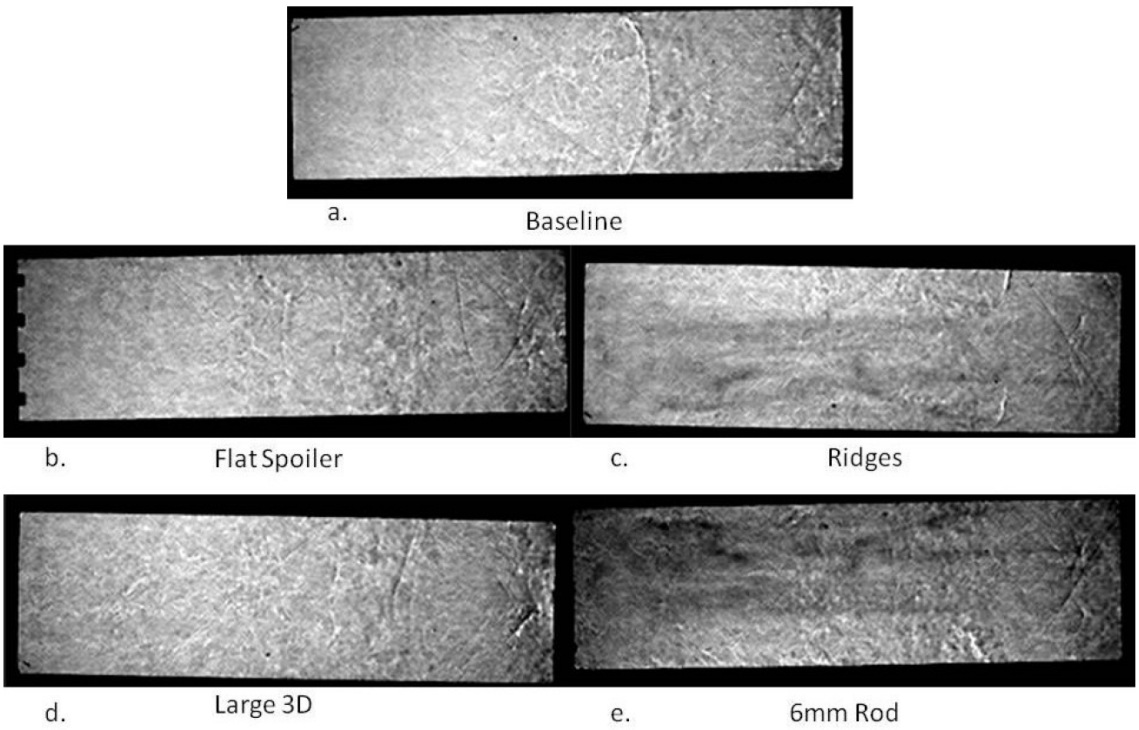

Figure 9 Shadowgraph Images of the side view a. Baseline, b. Large Backward Facing Steps, c. Ridges, d. Flat Spoiler, e. 6 mm Rod.

Figure 10 is shows the sketches of side and top views of the observable flow fields patterns for the various geometry modification tested. Figure 10 a and b are the baseline flow field patterns. The main flow features that are observable are the shear layer with distinct large vortices traversing the cavity and the bifurcated reticulating region in the aft of the cavity, these features have been discussed in Schmit et al.[6] but are here for comparison purposed. Figure 10 c and d shows the Ridges device flow pattern. The flow feature are very similar to the baseline in that the shear layer and the bifurcated recirculation region are nearly the same size and strength. Figure 10 e and f shows the flat spoiler flow pattern. This device attempts to loft the shear layer, but the shear layer growth is nearly the same. The bifurcated recirculation region is about half the size in the side view though it is nearly the same in the top view indicating that there is some change in the shear layer that is not easily observable at this time. Figure 10 g and h shows the large backward facing steps flow pattern. The shear layer is significantly different in that the shear layer starts below the waterline of the cavity and slightly dips further into the cavity and then back out and no large scale vortices are noticed in the shear layer. The recirculation region in the aft of the cavity is about the same size in the side view but looks a lot smaller in the top view. In the top side flow pattern several new features are observable, the streamwise vortices that are formed from the large backward facing steps. Figure 10 i and j shows the 6 mm rod flow pattern. The side view flow pattern is the most transformed. Since the rod sheds it own vortices the cavity shear layer is altered in such a way that no major vortices form inside the cavity shear layer and the large recirculation region in forward part of the cavity is formed. From the top view the only major flow field pattern that is observable is the shedding from post that hold up the rod.

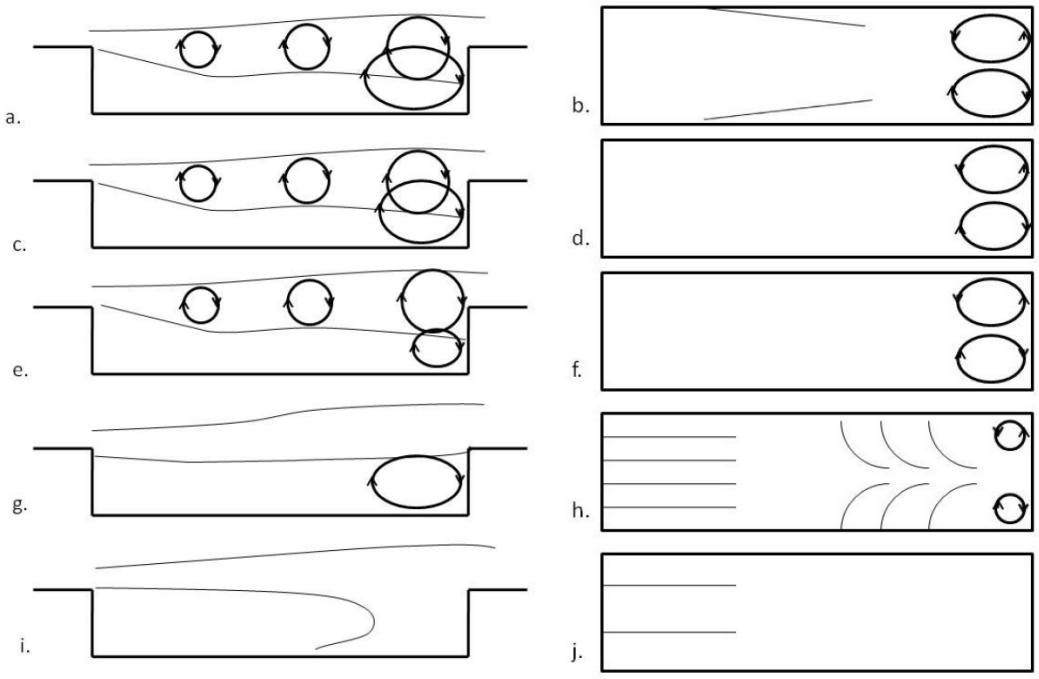

Figure 10: Schematic drawings of the side view and top view flow field patterns inside the cavity. a and b Baseline side view and top view, c and d. ridges device side and top view, e and f flat spoiler side and top view, g and h Large backward facing steps side and top view, i and j 6 mm Rod side and top view.

Figure 11 shows the combined results for the baseline. Again Schmit et al.[6] has more details on the baseline results and the current figure is used for comparison purposes. Figure 11 a and b show the DFT results of the high speed shadowgraph images for the side and top views, respectively at the peak acoustic frequency. The side results show that at the peak acoustic frequency the shear layer is the strongest feature in the flow field. The shocks have significant strength except they very little of the acoustic spectrum unlike the shear layer. The top side view shows some of the strongest density fluctuation at the peak acoustic frequency to be along side walls of the cavity as well as the aft wall indicating higher density flow is traveling forward along the side walls. The strong feature at the aft wall is from the high density vortices traveling down the aft wall of the cavity due to the aft recirculation region. Figure 11c shows the pressure spectrum along the ceiling of the cavity. The peak frequency is dominate throughout the cavity though it dips slightly near front wall. Other acoustic peak frequency are present as well throughout the cavity. Figure 11d shows the instantaneous pressure throughout the cavity. One feature that is noticeable is the pumping action in the cavity. Schmit et al.[6] gives more detail about the pumping action inside the cavity, but the penetration depth of the vortices dominated the pumping action. Figure 11e shows the cross correlation between the aft wall pressure senor and the pressure sensors in the ceiling of the cavity. This confirms that there are two recirculation regions in the cavity, the first is the aft recirculation region which is noticeable and the second dominate the rest of the cavity.

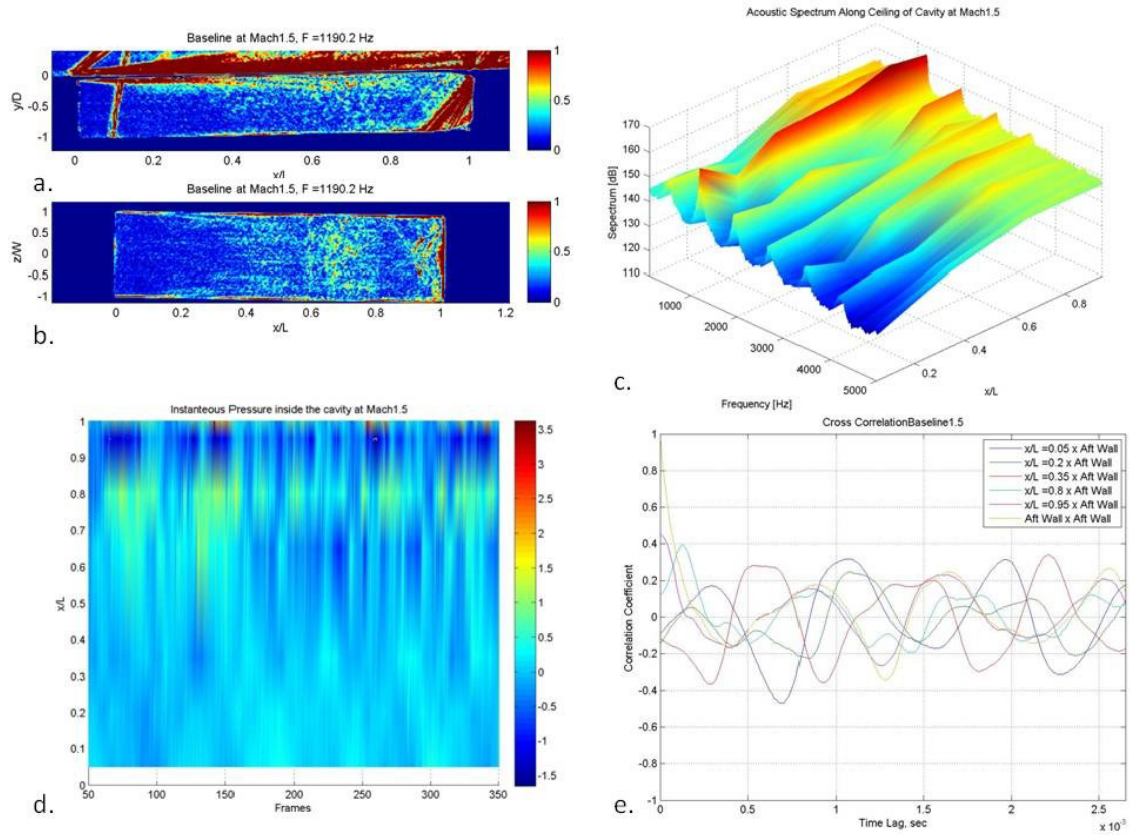

Figure 11: Baseline results a DFT of the side view, b DFT of the top view, e Acoustic Spectrum throughout the cavity, d Instantaneous pressure throughout the cavity, e Cross Correlation

Figure 12 shows the combined results for the Ridges device. Figure 12 a and b show the DFT results of the high speed shadowgraph images for the side and top views, respectively. The side results show that at the peak acoustic frequency the shear layer is the strongest feature in the flow field, thought they are not as strong as the baseline. The top side view shows that the strongest density fluctuations are along the aft walls of the cavity. Again the aft wall density is from the vortices traveling down the aft wall of the cavity do to the aft recirculation region. Figure 12c shows the pressure spectrum along the ceiling of the cavity. The peak frequency is dominate throughout the cavity though it dips slightly near front wall. Most of the other frequencies that are present in the baseline are not as observable. Figure 12d shows the instantaneous pressure throughout the cavity. The pumping action with the ridges is slightly more noticeable with this device indicating that the vortices are slightly stronger when they penetrate cavity. Figure 12e shows the cross correlation between the aft wall pressure senor and the pressure sensors in the ceiling of the cavity. Because the ridges device has one dominate tone the correlation is significantly higher than the baseline, though when examining each correlation shows that there is still two recirculation regions in the cavity.

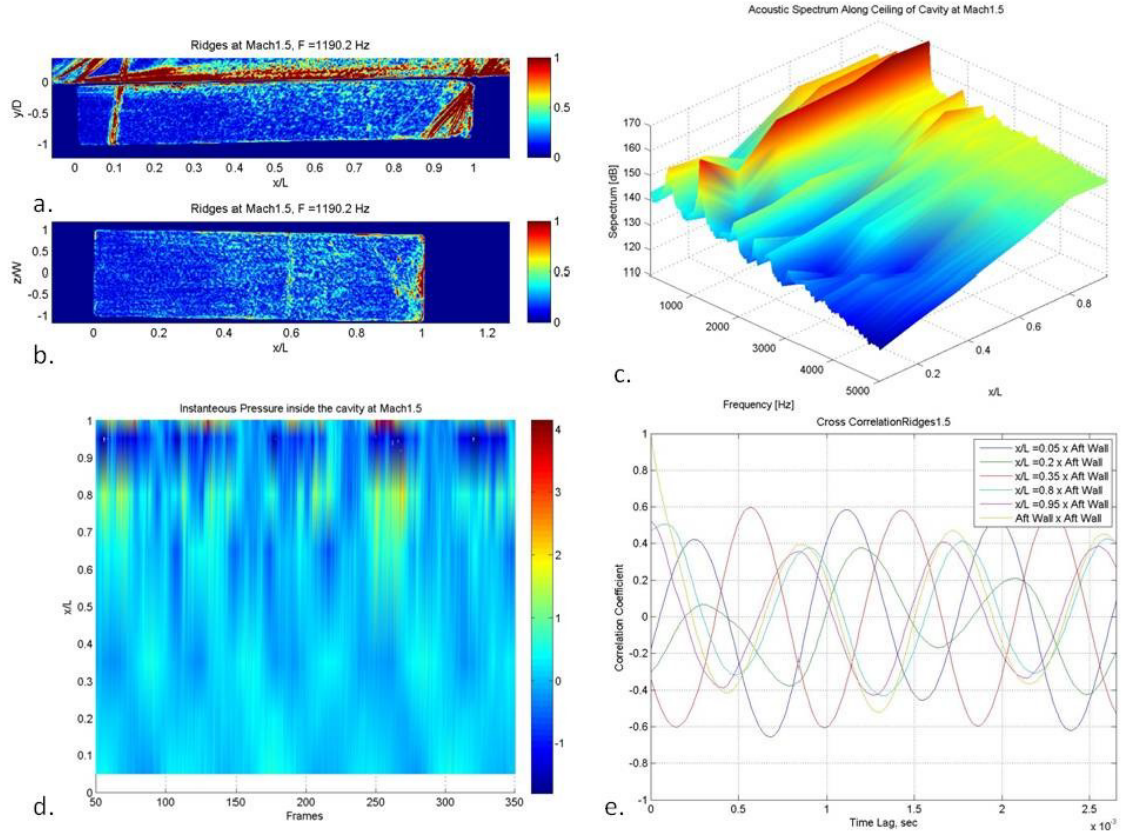

Figure 12: Ridges device results a DFT of the side view, b DFT of the top view, e Acoustic Spectrum throughout the cavity, d Instantaneous pressure throughout the cavity, e Cross Correlation

Figure 13 shows the combined results for the flat spoiler. Figure 13 a and b show the DFT results of the high speed shadowgraph images for the side and top views, respectively. Figure 13a is a zoomed out image of the flat spoiler and it still shows the similar trended in that shear layer is the strongest feature in the flow field but it is not as strong as the baseline. The top side view shows that the strongest density fluctuations are along the aft walls of the cavity. Again the aft wall density is from the vortices traveling down the aft wall of the cavity do to the aft recirculation region. Figure 13c shows the pressure spectrum along the ceiling of the cavity. The peak frequency is dominate throughout the cavity though it dips slightly near front wall. Most of the other frequencies are present like the baseline showing that the flat spoiler is not effective of lifting the shear layer over the entire cavity. Figure 13d shows the instantaneous pressure throughout the cavity. The pumping action is not as great considering that the fluctuations are at least 2 psi lower than all over conditions examined so far. Figure 13e shows the cross correlation between the aft wall pressure senor and the pressure sensors in the ceiling of the cavity. Again the cross correlation is similar to the baseline which not surprising since the flat spoiler has little effect.

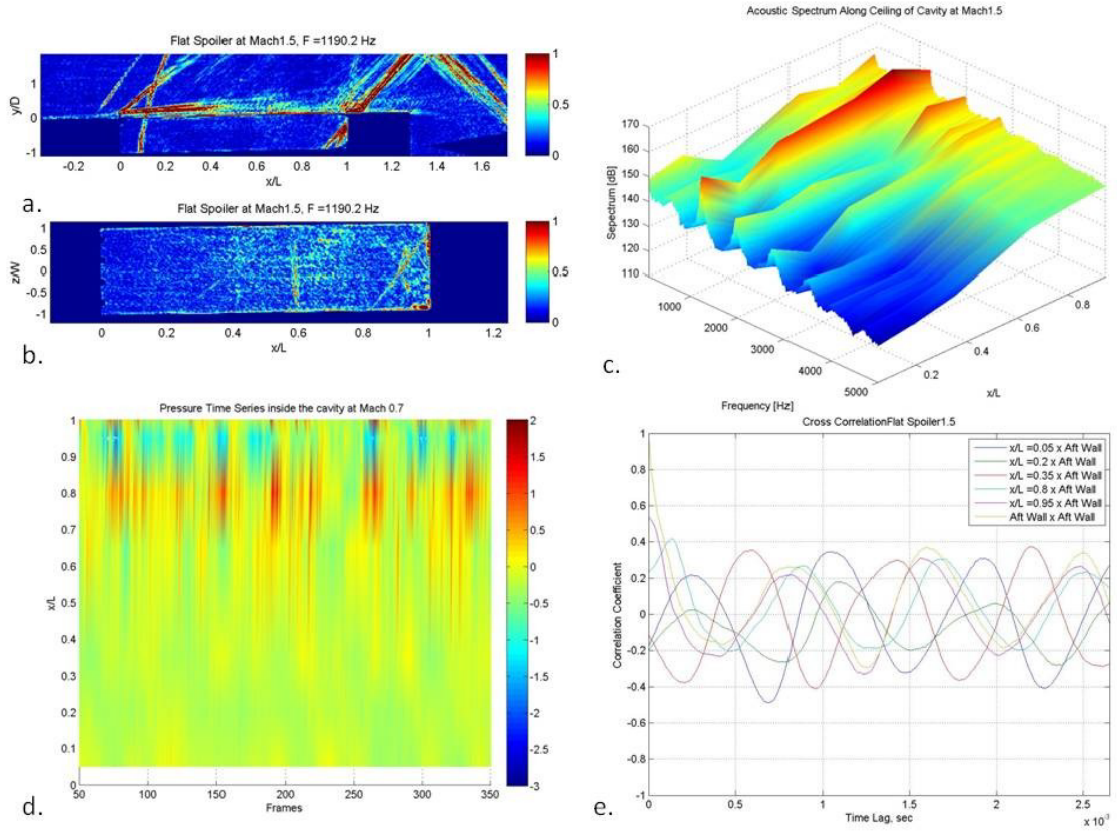

Figure 13: Flat Spoiler device results a DFT of the side view, b DFT of the top view, c Acoustic Spectrum throughout the cavity, d Instantaneous pressure throughout the cavity, e Cross Correlation

Figure 14 shows the combined results for the large backward facing step. Figure 14 a and b show the DFT results of the high speed shadowgraph images for the side and top views, respectively. The side view once again shows a similar trended in that shear layer is the strongest feature in the flow field but it is not as strong as the baseline. The top side view doesn't show the density fluctuations that travel down the aft wall of the cavity. Again the aft wall density is from the vortices traveling down the aft wall of the cavity do to the aft recirculation region. Figure 14c shows the pressure spectrum along the ceiling of the cavity. The peak frequency in the ceiling of the cavity is not at the dominate frequency that has been observed with all over device so far. The peak frequency is around 200 Hz which indicates the some other flow feature is creating the acoustic peak since it doesn't traverse the entire cavity. Figure 14d shows the instantaneous pressure throughout the cavity. The pressure fluctuations are not as great throughout the cavity since no vortices are being formed to penetrate the cavity depths to create the pumping action. Figure 14e shows the cross correlation between the aft wall pressure senor and the pressure sensors in the ceiling of the cavity. With the larger backward facing step there is virtually no correlation between any of the sensors which is indicative of a large recirculation region in the front of the cavity.

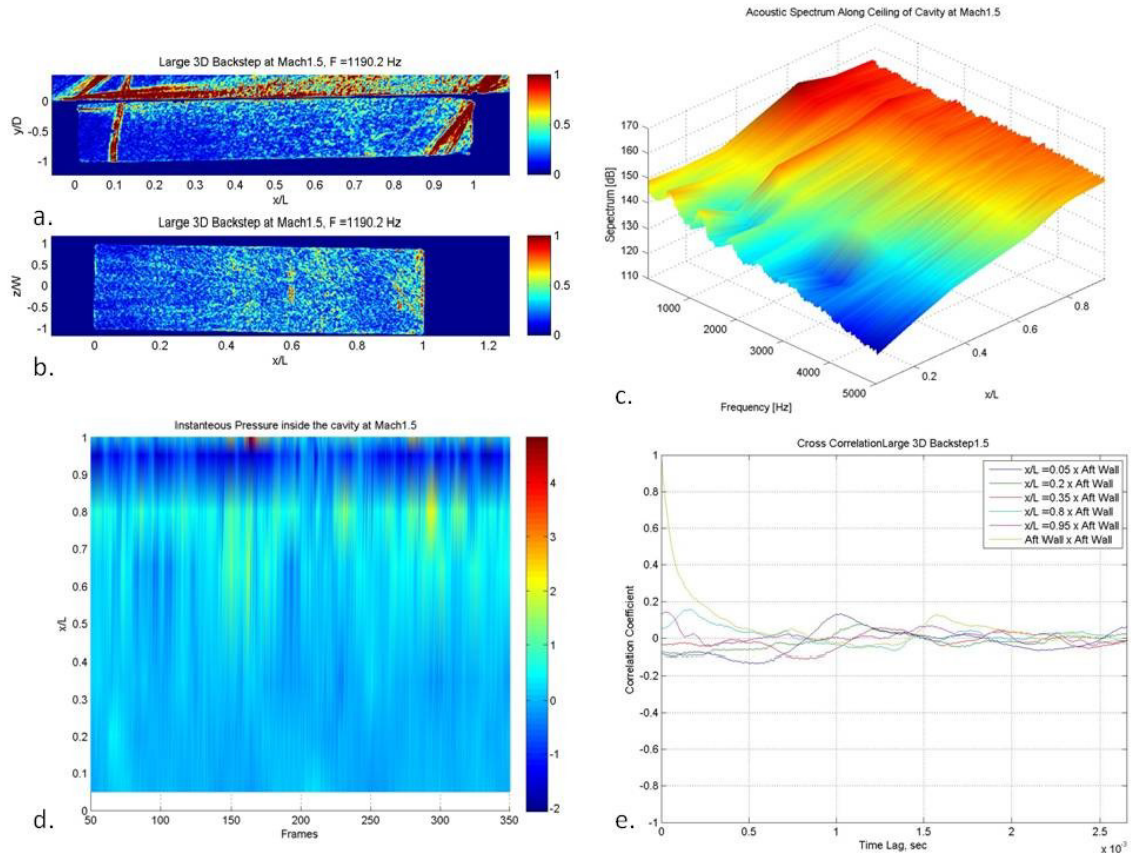

Figure 14: Flat Spoiler device results a DFT of the side view, b DFT of the top view, c Acoustic Spectrum throughout the cavity, d Instantaneous pressure throughout the cavity, e Cross Correlation

Figure 15 shows the combined results for the 6 mm rod. Figure 15 a and b show the DFT results of the high speed shadowgraph images for the side and top views, respectively. The side view shows that the shear layer is not dominate at the baseline's dominate frequency. The top side view doesn't show the density fluctuations that travel down the aft wall of the cavity. Again the aft wall density is from the vortices traveling down the aft wall of the cavity do to the aft recirculation region. Figure 15c shows the pressure spectrum along the ceiling of the cavity. The peak frequency in the ceiling of the cavity is not at the dominate frequency that has been observed with all other devices but is around 200 Hz which indicates a larger recirculation regions. Figure 15d shows the instantaneous pressure throughout the cavity. The pressure fluctuations are not as great throughout the cavity since no large scale vortices are being formed even though they are penetrating the cavity. Figure 15e shows the cross correlation between the aft wall pressure senor and the pressure sensors in the ceiling of the cavity. As with the larger backward facing step, there is virtually no correlation between any of the sensors because of the larger recirculation region that spans most of the cavity

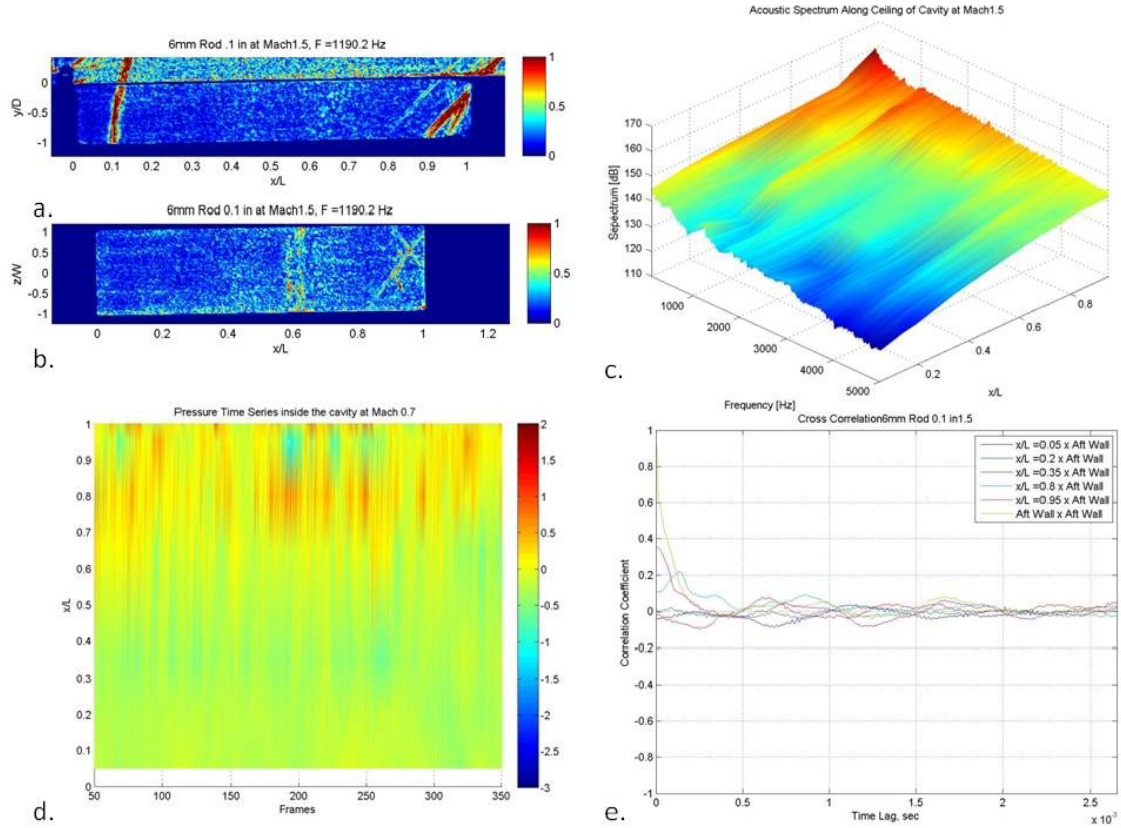

Figure 15: 6 mm Rod results a DFT of the side view, b DFT of the top view, e Acoustic Spectrum throughout the cavity, d Instantaneous pressure throughout the cavity, e Cross Correlation

Figure 16 shows the DFT results in the top view for the baseline and the four flow control devices tested. Figure 16 a and b are the same as Figure 11b and 12b, respectively and are shown again just for comparison. Figure 16c is the Ridges device at 1135 Hz and streaks can be seen in the front of the cavity and are produced by the streamwise vortices that are formed from the device. The frequency at which the streaks are produced might contribute to the increase in the peak acoustic tone from this device. Figure 16d is the large backward facing steps at 274 Hz. Again streak are observable from the streamwise vortices that are produced. The larger spacing and streamwise vortex size provide longitudinal stability to the shear layer and keep the shear layer from producing large scale vortices that entrain freestream flow into the cavity. Figure 16e shows the 6 mm Rod at 183 Hz. Two streaks are shown near the front of the cavity. These two streaks are the corner vortices at are produced from the post that support the rod and may not provide any stability to the shear layer since most of the shedding from the rod reduces the formation of large shear layer vortices.

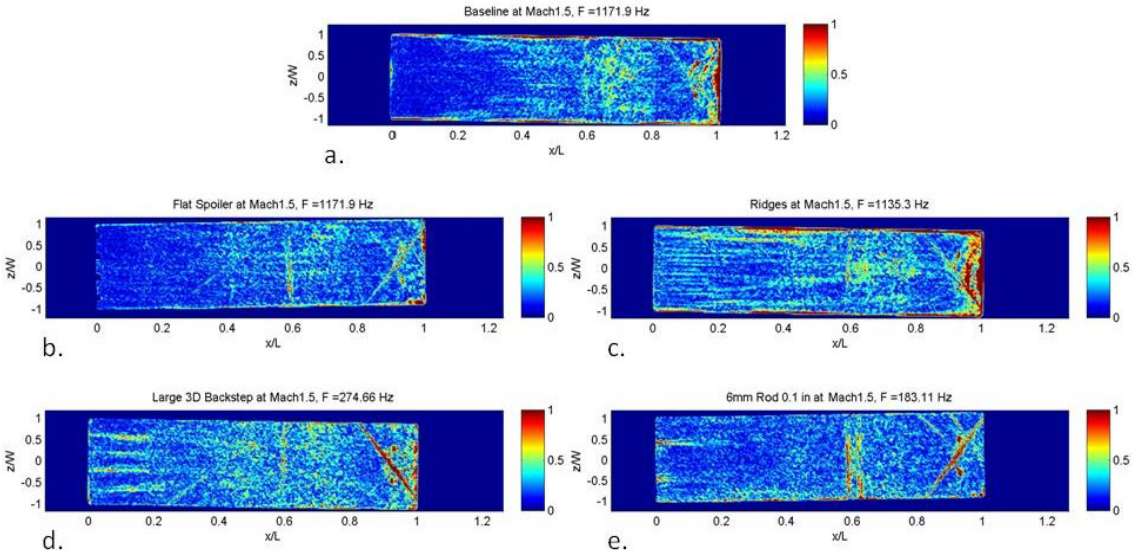

Figure 16: Top view of the DFT results at different dominate frequency

IV Conclusions

Reducing the acoustic tones and broadband noise inside a cavity within a supersonic flow field is more difficult than with a subsonic flow field. The correct passive flow control device can be effective at controlling the flow field inside the cavity, but the effectiveness at reducing the acoustic tones and broadband noise decreases when the flow conditions become supersonic. When passive flow control devices are tested supersonically, the behavior is very similar to the subsonic conditions previously tested. The one noticeable difference between the subsonic and supersonic conditions is that density fluctuations in the flow field are more observable in the shadowgraphs images in supersonic conditions.

Flow control device design for the cavity is critical in that the results from ridges device shows that even when streamwise vortices are introduced into the cavity, the flow control device can intensify acoustic tones. When streamwise vortices are introduced into the cavity, e.g. with backward facing steps with the correct spacing, they can be effective at reducing the acoustic tones by reducing the amount of flow entrained into the cavity. Even the rod in crossflow at supersonic conditions was not as effective at reducing the acoustic tones as it was in the subsonic case. One possible reason is that the shedding from the rod is directed more into the cavity supersonically than it is subsonically, which would result in more flow entrained into the cavity which enhances acoustic wave formation inside the cavity.

To develop an effective flow control device for supersonic conditions, so that it can lower the peak acoustic tone as well as the broadband noise, it has to be designed correctly. Stabilizing the shear layer with streamwise vortices is one method that may work, thought the correct vortex spacing is needed. Lofting the shear layer is extremely hard to do supersonically, so limiting the amount of fluid entrained into the cavity is probably the next best thing to do. Even a small amount of fluid entrained into the cavity can initiate the acoustic cycle inside the cavity, as seen with the rod in the cross flow.

References

[1]Rossiter, J. E., "Wind-Tunnel Experiments on the Flow over Rectangular Cavities at Subsonic and Transonic Speeds" London: Ministry of Aviation, Report and Memoranda No. 3438, 1966.
[2]Heller, H. H., and Bliss, D., "The Physical Mechanism of Flow-Induced Pressure Fluctuations in Cavities and Concepts of their Suppression," AIAA paper 75-491, 2nd Aeroacoustic Conference, Hampton VA 1975
[3]Tam, C. K., and Block, P. J, "On the Tones and Pressure Oscillations induced by Flow Over Rectangular Caviteis," *Journal of Fluid Mechanics*, Vol 89 (part 2), 1978, pp. 373-399.

[4]Zhuang, N., Alvi, F. S., Alkislar, M. B., and Shih, C., "Supersonic Cavity Flows and Their Control," *AIAA Journal*, Vol 44, No. 9, Sep. 2006, pp. 2118-2128.
[5]Moon, S. J., Gai, S. L., Kleine, H. H., and Neely, A. J., "Supersonic Flow Over Straight Shallow Caviies In Leading and Trailing Edge Modification," *28th AIAA Applied Aerodynamic Conference*, Chicago IL, 2010, pp. 1-11, AIAA 2010-4687
[6]Schmit, R.. F., Semmelmayer, F., Haverkamp, M.., and Grove, J., "Fourier Analysis of High Speed Shadowgraph Images around a Mach 1.5 Cavity Flow Field", *29th AIAA Applied Aerodynamic Conference*, Honolulu, HI, 2011, pp. 1-24, AIAA 2011-3961
[7]Rizzetta, D. P., and Visbal, M. R., "Large-Eddy simulation of superonic cavity flow-fields including flow control," *AIAA Journal*, Vol. 41, No. 8, Aug. 2003, pp. 1452-1462.
[8]Peng, S.-H., "Simulation of Turblent Flow Past a Rectangluar Open Cavity Using DES and Unsteady RANS," *24th AIAA Applied Aerodaynmaics Conference*, San Francisco, CA, 2006, pp. 1-20, AIAA 2006-2827
[9]Li, W., Nonomura, T., and Fujii, K., "Effects of shear-layer charateristic on the Feedback-loop Mechanism in supersonic open cavity flows," *49th AIAA Aerospace Sciences Meeting including the New Horizons Forum and Aerospace Exposition*, Orlando, FL, 2011, pp. 1- 12, AIAA 2011-1218
[10]Murray, N., and Ukeiley, L. "An application in Gappy POD", *Experiments in Fluids* Vol 42, No. 1, Jan. 2007, pp. 79-91.
[11]Dudley, J. G., and Ukeiley, L. "Suppresion of Fluctuating Surface Pressure in a Supersonic Cavity Flow," *5th Flow Control Conference*, Chicago, IL, 2010, pp. 1-22, AIAA 2010-4974
[12]Koschatzky, V., Westerweel, J., and Boersma, B. J., "Comparison of two ascostic analogies applied experimental PIV data for cavity sound emission estimation," *16th AIAA/CEAS Aeroacoustic Conference,* 2010, pp. 1-11, AIAA 2010-3812.
[13]Cattafesta, L., N., Song, Q., Willimas, D., R., Rowley, C., W., and Alvi, F., S.,"Active Control of Flow-Induced Cavity Oscillations," Progress in Aerospace Sciences, Vol. 44, 2008, pp. 479-502
[14] Schmit, R.F., Semmelmayer, F., Haverkamp, M., Grove J. E., and Ahmed A., "Analysis of Cavity Passive Flow Control using High Speed Shadowgraph Images", *50th Aerospace Sciences Meeting Including the New Horizons Fourm and Aerospace Exposistion*, 2012, pp 1-17, AIAA 2012-0738
[15]Clark, G. F. "Trisonic Gasdynamic Facility User Manual," Air Force Wright Aeronautical Laboratories Wright-Patterson AFB, AFWAL-TM-82-176-FIMM, 1982.
[16]Kaufman, L. G. and Clark, R. L. "Mach 0.6 to 3.0 Flows Over Rectangular Cavities," Air Force Wright Aeronautical Laboratories, Wright-Patterson AFB, AFWAL-TR-82-3112, 1983.
[17]Dussauge, J. P, Smits A J., 1997, "Characteristic scales for energetic eddies in turbulent supersonic boundary layers," *Experimental Thermal and Fluid Sciences*, Vol. 14, pp. 85-91
[18]Birch, S. L and Eggers, J. M., 1973, "A critical review of experimental data for developed free turbulent shear layers," NASA SP321, pp. 943-949
[19]Pantano, C. and Sarkar, S., "A study of compressibility effects in the high-speed turbulent shear layer using direct simulation" *Journal of Fluid Mechanics*, Vol 14 2002, pp. 329-371
[20]Clemens, N T., Mungal M G., 1995, Large-scale structures and entrainment in supersonic mixing layer, J. Fluid Mech., 248, pp. 171-16
[21]Lilley G M., 2008, The generation of sound in turbulent motion, Aeronautical Journal, 112, pp. 381-394
[22]Blumen W., Dazing P G., Billings D F., 1975, Shear layer instability of inviscid compressible fluid, Part 2. J. Fluid Mech., 71, pp. 305-316
[23]Papamoschou D., Roshko A., 1988, The compressible turbulent shear layer: an experimental study, J. Fluid Mech., 197, pp. 453-477
[24]Schulein E, Trofimov V M., 2011, Steady longitudinal vortices in supersonic turbulent separated flows. J. Fluid Mech. 672, pp. 451-476.
[25]Schmit, R. F., McGaha, C., Tekell, J., Grove, J., and Stanek, M., "Performance Results for the Optical Turbulence Reduction Cavity," *47th AIAA Aerospace Science Meeting Including the New Horizons Forum and Aerospace Exposistion*, Orlando FL, 2009, pp. 1-13, AIAA 2009-702
[26]Stanek, M. J., Visbal, M. R., Rizzetta, D. P., Rubin, S. G., and Khosla, P. K., "On A Mechanism of Stabilizing Turbuelent Free Shear Layers in Cavity Flows," *Computers & Fluids*, Vol 36, No 10 Dec 2007, pp 1621-1637.
[27]Zhang X., Rona A., Edwards J A., 1998, The effect of trailing edge geometry on cavity flow oscillations driven by a supersonic shear layer. Aeronautical Journal 3, pp. 129-136
[28]Bar G L., 1972, Experimental investigation of the sudden expansion of a supersonic plane flow into a 90°Vee channel. MS Thesis, Aerospace Engineering Department, Wichita State University, KS
[29]Ahmed, A., Zumwalt, G. W., 1993, Base Drag Reduction of a Non-Circular Missile, Journal of Spacecraft and Rockets, 30 (6) pp. 781-782
[30]Settles, G. S., *Schlieren and Shadowgraph Techniques: Visualizing Phenomena in Transparent Media* Springer, Berlin, 2006.